Multi-Channel Radio-Over-Fiber Communication Systems Through Modulation Instability Phenomenon

Rasul Azizpour, Hassan Zakeri, Gholamreza Moradi, *Senior Member, IEEE*, Mohammad Alibakhshikenari, *Member, IEEE*, Francisco Falcone, *Senior Member, IEEE*, BO Liu, *Senior Member, IEEE*, Tayeb A. Dendini, *Fellow, IEEE*, Imko Park, *Senior Member, IEEE*, Slawomir Koziel, *Fellow, IEEE*, and Ernesto Limiti, *Senior Member, IEEE*

***Abstract*—Recent advancements in Radio-over-Fiber (RoF) technology have positioned it as a promising solution for high-capacity wireless communications. This paper explores novel applications of RoF systems in enhancing phased array antenna (PAA) performance for multi-channel wireless communication applications through the modulation instability (MI) phenomenon. Utilizing fibers experiencing MI with varying group velocity dispersions (β_2) of -20, -11.3, -3.2, and -2 ps^2/km, the RoF system achieves operational flexibility across distinct central frequencies of 12, 16, 30, and 38 GHz, respectively. This approach represents a significant advancement in wireless communication technology, leveraging MI gain and an MI-based control system architecture to enhance performance across diverse frequency bands. The study investigates the impact of MI on modulation efficiency, presenting experimental results validating the feasibility and effectiveness of the proposed approach. The maximum MI gain by employing a 30 km fiber under MI is 18 dB, experimentally. Further optimization, achieved by increasing the fiber length to 45 km and adjusting nonlinear parameters and input power, demonstrates a remarkable MI gain of 38.1 dB. MI-based true time delay (TTD) techniques also address beam squint challenges, enhancing beamforming capabilities. The findings suggest that integrating MI into RoF systems holds excellent potential for improving wireless communication capabilities with reduced costs and space requirements compared to conventional methods. This research contributes to the growing body of knowledge in the field of RoF systems and offers insights into their practical applications in modern wireless communication networks.**

***Index Terms*—Modulation instability (MI), Mach-Zehnder modulator, phased array antenna, radio-over-fiber, wireless application.**

Manuscript received 21 June 2024; revised 26 July 2024; accepted 15 August 2024. Date of publication 20 August 2024; date of current version 11 September 2024. Mohammad Alibakhshikenari acknowledges support from the CONEX (CONnecting EXcellence)-Plus programme funded by Universidad Carlos III de Madrid and the European Union's Horizon 2020 research and innovation programme under the Marie Sklodowska-Curie grant agreement No. 801538. *(Corresponding authors: Mohammad Alibakhshikenari; Ernesto Limiti.)*

Rasul Azizpour, Hassan Zakeri, and Gholamreza Moradi are with the Microwave Measurement Research Laboratory, Department of Electrical Engineering, Amirkabir University of Technology (Tehran Polytechnic), Tehran 15875-4413, Iran (e-mail: ra.azizpour@aut.ac.ir; h.zakeri@aut.ac.ir; ghmoradi@aut.ac.ir).

Mohammad Alibakhshikenari is with the Department of Signal Theory and Communications, Universidad Carlos III de Madrid, 28911, Leganés Madrid, Spain (e-mail: mohammad.alibakhshikenari@uc3m.es).

Francisco Falcone is with the Department of Electrical, Electronic and Communication Engineering and Institute for Smart Cities (ISC), Public University of Navarre, 31006, Pamplona, Spain, and also with the School of Engineering and Sciences, Tecnologico de Monterrey, Monterrey 64849, Mexico (e-mail: francisco.falcone@unavarra.es).

BO Liu is with the James Watt School of Engineering, University of Glasgow, G12 8QQ Glasgow, U.K. (e-mail: bo.liu@glasgow.ac.uk).

Tayeb A. Dendini is with the Centre-Energie Matériaux et Télécommunications, Institut National de la Recherche Scientifique, Montreal, QC H5A 1K6, Canada (e-mail: denidni@emt.inrs.ca).

Imko Park is with the Department of Electrical and Computer Engineering, Ajou University, Suwon 16499, Republic of Korea (e-mail: ipark@ajou.ac.kr).

Slawomir Koziel is with the Faculty of Electronics, Telecommunication and Informatics, Gdańsk University of Technology, 80-233 Gdańsk, Poland, and also with the Department of Engineering, Reykjavik University, 102 Reykjavik, Iceland (e-mail: slakozie@pg.edu.pl).

Ernesto Limiti is with the Electronics Engineering Department, University of Rome "Tor Vergata", 00133 Rome, Italy (e-mail: limiti@ing.uniroma2.it).

Digital Object Identifier 10.1109/JPHOT.2024.3446314

I. Introduction

RoF technology has recently become one of the most well-known schemes for the forthcoming high-capacity wireless communications industry due to its benefits, including large bandwidth, cost efficiency, and reduced signal attenuation [1], [2]. Several methods have already been presented using this technique to provide multiple services for mobile and fixed users by utilizing the advantages of wired and wireless technologies [3], [4]. Due to the availability of dynamic spectrum allocation in wireless communication and the transparent carriage of analog or digital signals, RoF systems can be used in many radio-frequency (RF) bands [4], [5]. Many of these applications, such as new generation communication 5G/6G [6], [7], [8], [9], Internet of Things (IoT) [10], [11], supporting terahertz devices and antenna [12], [13], [14], and medical sensors [15] operate at RF bands. RoF technology integrates optical communication and wireless systems to provide long-distance transmission of wireless signals with reduced cost solutions and higher data rates due to its advantages, including immunity to RF interference, reduced power consumption, dynamic resource allocation, multi-operator, and multi-service. This technique integrates wireless systems with optical fiber infrastructure, distributing RF signals across multiple base stations (BSs) via optical fiber links [16], [17], [18], [19]. Despite these advantages, RoF systems are susceptible to phase noise, which originates from imperfections in oscillators and other electronic components. However, the

impact of phase noise on RoF systems can be managed and mitigated through various techniques, making it less detrimental than in different communication systems. Phase noise can degrade signal quality, increase bit error rates (BER), and cause leading to interference and crosstalk between channels. As a result, understanding and mitigating phase noise is essential to maintaining the performance and reliability of RoF systems [20], [21]. Advanced modulation formats [22], digital signal processing (DSP) [23], and high-quality oscillators [24] can significantly reduce the effects of phase noise in RoF systems. These methods help maintain signal integrity and ensure the reliable performance of RoF technology in modern communication networks. Modulators and photodetectors perform electrical-to-optical (EO) and optical-to-electrical (OE) transformations on the transmitting and receiving sides of the photonic link, respectively [25], [26].

The optical modulation process, a pivotal aspect of RoF systems, involves manipulating the properties of light to encode information onto optical carriers [27], [28]. This process can be achieved through various techniques, including the use of external modulators, such as an electro-absorption modulator or a Mach-Zehnder modulator (MZM). The features of MZM, like low harmonic distortion and high speed, make it an essential component in advancing coherent technology [29]. The half-wave voltage (V_π), which is an important MZM characteristic, is the voltage needed to cause a 180° (π radians) shift on the optical carrier as it travels through the MZM waveguide arms. Additionally, due to its connection to the design, manufacture, and packaging of the optical modulator and also the dependency of V_π to the frequency, it is necessary to evaluate the performance of optical modulators [30].

In the experimental case, critical elements, including impedance mismatching, plasmonic losses, and variations in microwave-optical velocities, lead to a drop in modulation flexibility with frequency. Furthermore, in the modes which has high-efficiency, the product of the arm length of EO modulators and modulation voltage remains constant ($V_\pi L = \alpha$). Consequently, the EO arm's length increases as V_π decreases. The modulation response declines faster with increasing frequency, leading to a decrease in the bandwidth. Consequently, in many cases, there is a direct proportionality between the modulators' V_π and bandwidth [31], [32], [33].

Recently, electronic devices have decreased their output voltage by increasing frequency, aiming to enhance modulation efficiency. However, in modulator devices like MZMs, this strategy contradicts the desired effect of high frequency on maintaining a constant V_π. Various techniques, including the utilization of novel materials [34], have been investigated to improve the effectiveness of V_π. However, these approaches often introduce complexities and elevate costs associated with modulator design. Furthermore, endeavors aimed at reducing V_π by integrating various resonators and refining electro-optic circuitry have resulted in intricate structures that are highly susceptible to fabrication intricacies [35], [36], [37]. Additionally, the resonant characteristics of these structures may induce fluctuations in modulation response within the sideband spectrum, potentially distorting the output signal. Hence, the pursuit of enhancing V_π presents a challenging endeavor demanding innovative methodologies and solutions.

On the other hand, beamforming and gain enhancement stand as indispensable and challenging components in modern wireless communication systems, especially with the evolution of PAA. These techniques are instrumental in shaping the directionality of signals, thus enabling efficient transmission and reception in diverse environments [38]. The PAA system can focus its radiation pattern toward specific directions through beamforming, allowing for improved signal strength and reduced interference. Gain enhancement techniques amplify the transmitted signals and improve the overall system performance by increasing the SNR and extending the communication range [39], [40]. Furthermore, beam control mechanisms enable adaptive steering of the beams, optimizing the coverage and capacity of the communication network while mitigating the effects of multipath propagation and signal attenuation [41], [42].

Traditionally, electrical phase shifters have been used to control beam direction, which has some disadvantages such as limited steering resolution, frequency dependency, complexity and cost, sensitivity to environmental factors, and potential phase coherence issues [43]. New developments in true-time-delay (TTD) employing frequency comb (FC) technology offer an improved alternative to traditional techniques. In contrast to single-mode-fiber (SMF) based methods, which employ multiple fibers to supply an M-element PAA [44], [45], TTD with FC provides accurate and programmable time delays using just a single fiber, making it possible to achieve highly precise beam steering [46], [47].

The modulation instability (MI) phenomenon is a significant nonlinearity observed in optical fibers, owing to its role in producing soliton pulses and super-continuum generation. Numerous studies have explored MI, such as beam laser control [48], crystal fiber [49], rogue waves analysis [50], polarization control [51], and optical soliton [52], none have ventured into the realm of wireless communication applications utilizing microwave photonic technology. These investigations predominantly focus on terahertz frequencies within the fields of physics and optical applications.

The MI phenomenon, induced by altering the optical fiber's structure, increases power within the sidebands of the carrier signal, thereby enhancing the RF signal for antenna transmission. Employing FC based on TTD can facilitate PAA systems, where each comb drives a single element, ensuring all elements benefit from MI gain. The adoption of TTD effectively addresses the challenge of beamforming.

This paper presents a novel method of utilization of the MI phenomenon in RoF systems, addressing the challenges previously discussed. Our research aims to implement PAA systems by integrating MI-based gain enhancement and TTD techniques into RoF systems to be performed over a multi-frequency band, benefiting wireless communication systems over a wide frequency range. The utilization of MI in fiber optics has led to enhancements in the effective half-wave voltage ($V_{\pi,eff}$). Consequently, MI gain helps simplify the modulator's structure by discarding additional pumps, saving the input

power consumption, and reducing the shot noise effect caused by the photodetector, which improves wireless communication links.

Our experimental results agree with the simulation, confirming the feasibility of our approach in achieving advanced microwave and RF signal processing capabilities with the potential for reduced costs and space requirements compared to alternative solutions. The simulations were conducted using Optisystem software, which can perform Monte Carlo simulations to analyze the statistical variation in RoF system performance due to factors such as optical noise, fiber imperfections, and component variability.

The rest of the paper is structured as follows: Section II examines the MI phenomenon in optical fibers, including its gain and its impact on V_π. Section III presents the proposed RoF system architecture for different wireless communication frequency bands. Section IV discusses the detailed control system architecture within the RoF system, addressing both MI phenomenon and beam pattern management. In Section V, TTD-based beamforming techniques are explored, highlighting their advantages over traditional methods. Section VI investigates the use of MI to generate a boosted FC and its implications for RoF system performance. Section VII focuses on SNR in the proposed system, and finally, Section VIII concludes the paper by summarizing key findings.

II. Modulation Instability in Fiber Optic

MI is one of the most interesting phenomena in studying nonlinear waves. MI dynamics are linked to energy exchange between a continuous background and a periodic perturbation. In optical fiber systems, MI often occurs due to the interplay between the Kerr effect, dispersion, and non-linearity [53]. The intensity modulation induced by the Kerr effect can interact with dispersion to produce sidebands in the optical spectrum, leading to the onset of MI. As a third-order nonlinear process, the Kerr effect causes four-wave mixing between the frequency components of optical signals. This phenomenon results in a symmetrical frequency band centered around a specific frequency due to the conservation of photon energy $\hbar w$. Additionally, the conservation of photon momentum $\hbar\beta(w)$ dictates that only even components of the propagation constant contribute to the phase-matching condition [54], [55]. The effects of fiber dispersion are compensated for by expanding the mode-propagation constant in a Taylor series around the central frequency w_0 when $w = w_0 + \Omega$ (Ω is the frequency detuning), which is as follows:

$$\beta(w_0 + \Omega) = \beta_0 + \sum_{m=1}^{\infty} \frac{\beta_m}{m!}(\Omega)^m = \beta_0 + \delta\beta_e + \delta\beta_o \quad (1)$$

where $\beta_0 = \beta(w_0)$ denotes the propagation constant at the central frequency, while $\delta\beta_e$ and $\delta\beta_o$ represent the even and odd parts of the dispersion relation, respectively.

It's worth highlighting that $\delta\beta_e$ plays an essential role in the process of the Kerr effect. When employing standard SMFs in the C-band, the group velocity dispersion β_2 is dominant, rendering the higher-order coefficients negligible. Hence, $\delta\beta_e = \frac{\beta_2}{2}\Omega^2$.

Under the slowly varying envelope approximation, the unidirectional propagation of nonlinear waves, including optics, is described by the one-dimensional nonlinear Schrödinger equation (NLSE). This slowly-varying envelope $U(z,t)$ normalized to the input peak power (P_0) along the fiber, traveling with the group velocity $v_g = 1/\beta_1$, where $T = 1 - \beta_1 z$ is described by using the NLSE as follows [56]:

$$\imath\frac{\partial U}{\partial z} + \imath\frac{\alpha}{2}U - \frac{\beta_2}{2}\frac{\partial^2 U}{\partial T^2} + P_0\gamma\left|U\right|^2 U = 0 \quad (2)$$

where γ, β_2, and α are the nonlinear coefficients due to the Kerr effect, group velocity dispersion coefficient, and the fiber power attenuation coefficient, respectively.

Equation (2) can be easily solved by neglecting the time derivation to produce the steady-state continuous radiation solution. The continuous wave described by this equation exhibits a soliton form when the laser's response is lossless [56], [57]. A soliton refers to any optical field that remains unchanged along propagation due to an ideal balance between nonlinear and linear effects in the medium [58].

In a conventional RoF system, the group velocity dispersion of the fiber typically is positive ($\beta_2 > 0$), resulting in a real wave number (K) and a stable steady state that withstands small perturbations. Conversely, a negative group velocity dispersion ($\beta_2 < 0$) yields an imaginary wave number, amplifying perturbations. This parameter is a key factor in determining the operating frequency. In the scenarios where the interplay between nonlinearity and negative group velocity dispersion ($\beta_2 < 0$) coincide in a fiber, MI results. Consequently, the carrier sideband experiences amplification. A notable advantage of such a system lies in its capability to amplify the input pulse when modulated at the desired frequency.

A. Analytical Expression of the MI Gain

The linear stability analysis, whose derivation is based on the signal-idler technique used in optical parametric amplification (OPA), is applied to the NLSE to derive the MI gain. Assume the m and p denote the signal and idler or the Stokes and anti-Stokes components around the pump frequency. By employing the linear stability analysis, it obtained that the signal at fiber position L is given by $m(L) = m(0)A(L) + p(0)B(L)$. A and B are the signal and idler field gains, which are given by [56], [59]:

$$A(L) = \cosh(Lg) + i\frac{\Delta\beta/2 + \gamma P_0}{g}\sinh(Lg) \quad (3)$$

$$B(L) = i\frac{\gamma P_0}{g}\sinh(Lg) \quad (4)$$

where P_0, γ, and $\Delta\beta$ are the input pump power, the nonlinear coefficient, and the linear phase mismatch. The signal gain G_S is achieved by replacing the initial conditions $m(0) = 1$ and $p(0) = 0$ on the field so that $m(L) = A(L)$ and thus:

$$G_s = |m(L)|^2 = 1 + \left(\frac{\gamma P_0}{g}\right)^2 \sinh^2(Lg) \quad (5)$$

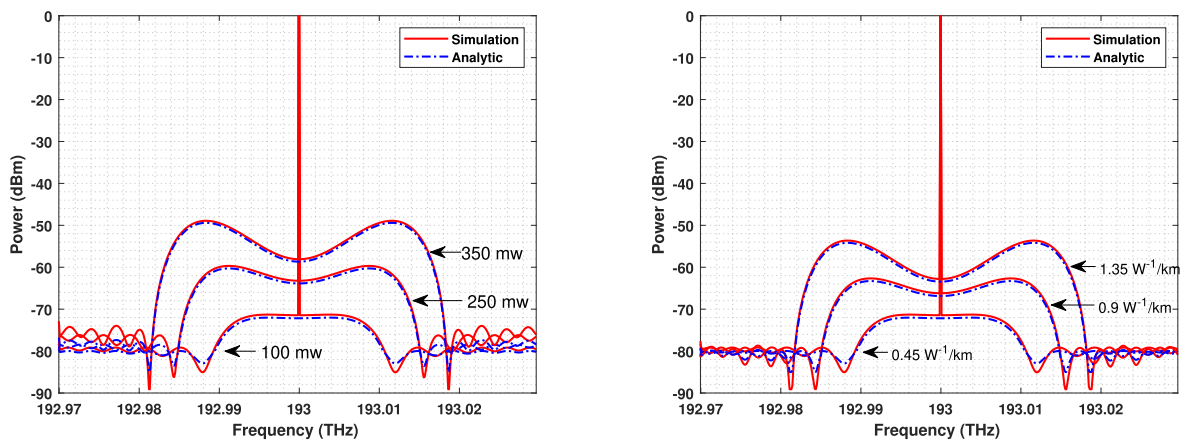

(a) (b)

Fig. 1. MI gain spectrum through a 45 km SMF with $\beta_2 = -20$ ps^2/km for (a) different values of input power and nonlinear parameter γ at 0.45 W^{-1}/km and under (b) different values of nonlinear coefficient and typical power values of 100 mw.

It is important to note that, the idler gain G_I is obtained by applying $m(0) = 0$ and $p(0) = 1$ on the field evolution leading to $m(L) = B(L)$ and therefore:

$$G_I = |m(L)|^2 = \left(\frac{\gamma P_0}{g}\right)^2 \sinh^2(Lg) \tag{6}$$

Since background noise operates as both a signal and an idler for MI, random variables can represent the beginning conditions. In this case, the Stokes and anti-Stokes components have the same intensity, which we set equal to unity to calculate gains because it is presupposed that the noise is white. The final gain value is the incoherent summation of the G_I and G_S when the signal and initial idler are white noises. Therefore:

$$G_{MI} = G_s + G_I = 1 + 2\left(\frac{\gamma P_0}{g}\right)^2 \sinh^2(Lg) \tag{7}$$

where L is the fiber length and the parametric gain coefficient g is defined as:

$$g^2 = -\Delta\beta(\gamma P_0 + \Delta\beta/4) \tag{8}$$

which $\Delta\beta$ denotes the linear phase mismatch between the pump, signal, and idler. Note that g can take a real or imaginary value, depending on the sign of the phase mismatch $\Delta\beta$. For standard SMFs at 1550 nm, $\Delta\beta$ can be expressed as $\beta_2\Omega^2$, where $\Omega = \omega - \omega_0$ is the frequency shift around the pump frequency ω_0 and β_2 is a principal characteristic of the anomalous fiber.

The maximum MI gain (G_{max}) happens at frequency shift of $\Omega_{max} = \pm\frac{\Omega_c}{\sqrt{2}} = \sqrt{\frac{2\gamma P_0}{|\beta_2|}}$. Regarding (9), this amplification is related to the frequency, carrier power, and fiber parameters (β_2 and γ).

$$G_{max} = \Omega_c^2|\beta_2|L = 4\gamma P_0 L \tag{9}$$

A nonlinear fiber with a specified design and under MI amplifies a particular spectral range of the carrier sideband by nonlinear frequency variation on the carrier. The amplification can be applied without a separate pump using the anomalous fiber [14], [60]. Moreover, in certain long-distance wireless applications, the signal received by the receiver may exhibit a lower amplitude than the transmitted signal. Consequently, this technique enables the amplification and detection of weak signals [61], [62].

In Fig. 1(a), the MI gain spectrum is presented for a SMF across different input power of 100, 250, and 350 mW and Fig. 1(b) shows the MI gain spectrum for different non-linear coefficient of 0.45, 0.9, and 1.35 W^{-1}/km. The analytical results are given directly from the MI gain equation in (7), and the simulation results have been obtained by employing OptiSystem, a widely recognized software tool for designing and analyzing optical communication systems.

The small difference between simulation and theory observed outside the carrier sideband is caused by the higher-order MI [63], [64], which is only present at very high power levels (above the typical power regime used in optical fiber systems) and is neglected in the analytical model.

Fig. 2 illustrates the amplification of carrier sidebands across varying fiber lengths and group velocity dispersion coefficients. Increasing the fiber length under MI amplifies MI gain, with the maximum gain rising from 10.5 dB to 31 dB as the fiber length increases from 15 km to 45 km. On the other hand, the variation in β_2 can solely change the amplification frequency range. In this scenario (Fig. 2(b)), the central frequencies of the sidebands at 7 GHz and 14 GHz can be amplified by employing fibers with group velocity dispersion of $\beta_2 = -36$ ps^2/km and -9 ps^2/km, respectively. Unlike altering the power and nonlinear characteristics of the fiber under MI (as shown in Fig. 1), tuning the length (L) and β_2 of the fiber (as shown in Fig. 2) to define the desired gain and frequency, respectively, can be an effective strategy to be used in microwave-photonic systems. Consequently, this technique can be utilized to improve the efficiency of wireless communication systems across various frequency bands.

Fig. 3 shows the amplification of the input signal (Gaussian pulse) with a central frequency of 12 GHz by different fiber lengths of 15 km, 30 km, and 45 km, respectively. In this case, the -6 dBm unboosted input signal is amplified at the carrier sideband. Increasing the length of the fiber results in a higher

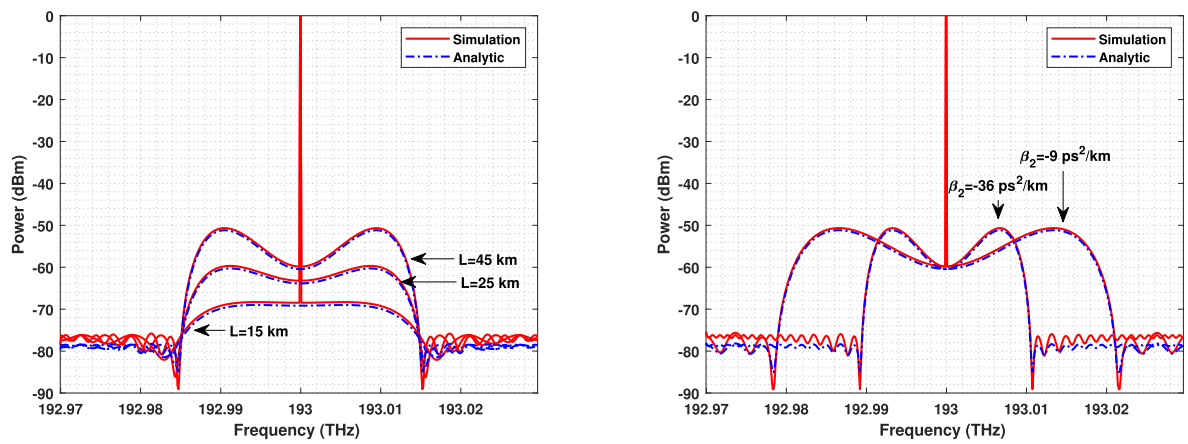

Fig. 2. MI gain spectrum with power level of 200 mw and $\gamma = 0.88\ W^{-1}/km$ for (a) different length of fiber with $\beta_2 = -20$ ps^2/km and for (b) different values of β_2 with fiber length of 45 km.

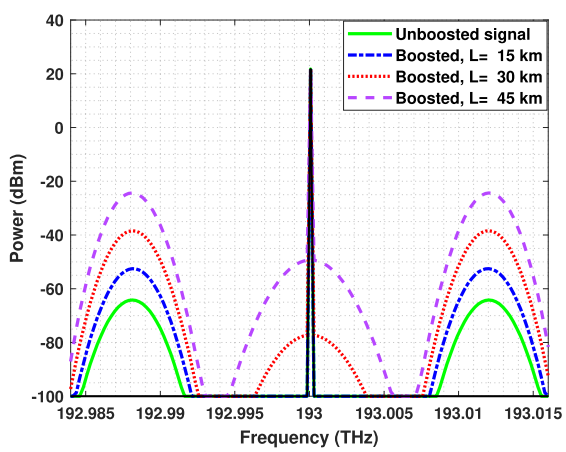

Fig. 3. Unboosted and boosted input Gaussian pulses with a central frequency of 12 GHz.

MI gain at the sideband carrier. The amount of maximum MI gain in the fiber lengths of 15 km, 30 km, and 45 km is 12.6 dB, 26.7 dB, and 38.1 dB, respectively. Therefore, the signal power increased to -25.9 dBm when using a 45 km fiber. The group velocity dispersion and the nonlinear refraction index of fiber are $\beta_2 = -20$ ps^2/km and $\gamma = 0.88\ W^{-1}/km$, respectively. Also, the carrier frequency and the input power are 193 THz and 250 mw, respectively.

B. V_π Challenge in Mach-Zehnder Modulator

Increasing the V_π with regards to raising the frequency is one of the critical challenges in designing broadband traveling-wave modulators like MZM that have approved performance. However, this ratio is inverse in electrical technology, such as devices that use CMOS [65]. Using the MZM in the proposed structure makes it possible to modulate the Gaussian pulse on the carrier. The transfer function for the MZM with an electro-optic element inserted in one arm creates a general method to evaluate EO modulation [56]:

$$P_{out} = \left(\frac{P_{in}}{2}\right)\left(1 + \cos\left(\phi_0 + \pi\left(\frac{v}{v_\pi}\right)\right)\right) \tag{10}$$

This represents the typical voltage change necessary to cause the phase shift between the modulator arms. Sideband fields rise by $G_{MI}^{1/2}$ where G_{MI} is the MI gain. The square of $G_{MI}^{1/2}$ is directly proportional to the RF output power, resulting in the following:

$$P_{out} \propto \left(\frac{1}{v_\pi^2}\right) P_{in} G_{MI} \tag{11}$$

With respect to (11) the raise of P_{out} by G_{MI} is equivalent to a V_π reduction by $G_{MI}^{1/2}$, therefore the improved half-wave voltage is achieved:

$$V_{\pi,eff}(\omega_{RF}) = V_\pi(\omega_{RF}) \frac{L_{Dep}^{1/2}}{G_{MI}^{1/2}(\omega_{RF})} \tag{12}$$

In this equation, $L_{Dep}^{1/2} < 1$ is the consumption factor for the power carrier. The effective half wave voltage $V_{\pi,eff}$ is decreased by utilizing the G_{MI} in the sideband, which helps to overcome the V_π challenge.

This configuration offers an advantage by enhancing the MI gain in the carrier's sideband, thereby improving the V_π of the MZM. In communication applications involving transmission and reception, boosting the modulator's gain enhances its performance, consequently reducing $V_{\pi,eff}$ and facilitating better detection of the received signal.

III. Proposed MI-Based RoF System

Fig. 4 illustrates the proposed MI-based RoF system. This system offers multi-channel RF tunable microwave TTD lines for PAAs utilizing an integrated on-chip micro-ring resonator (MRR) optical FC source. The generation of a broadband Kerr comb featuring numerous comb lines enables the feeding of PAAs with a large number of elements. By programming and

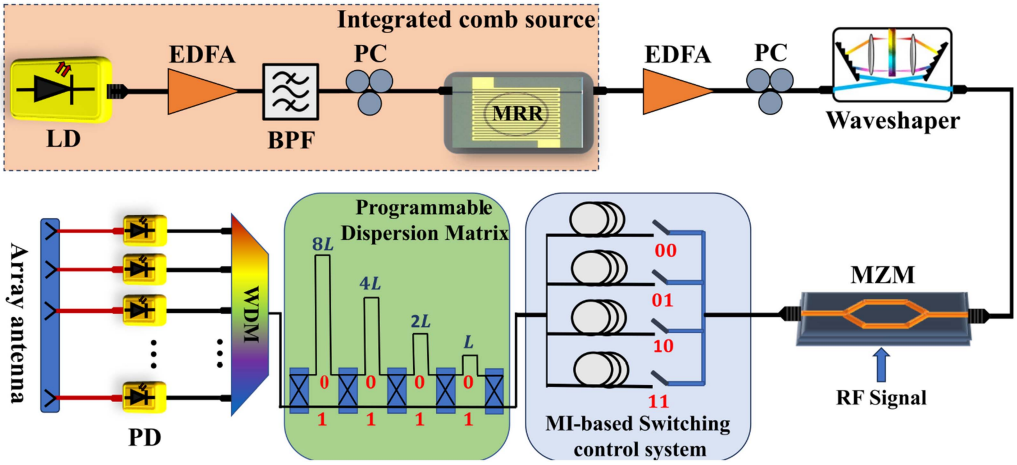

Fig. 4. Schematic diagram of the TTD device based on an integrated optical comb source. LD: laser diode, BPF: optical bandpass filter for optics application, PC: polarization controller, MRR: Micro ring resonator, WDM: wavelength division multiplexer. PD: photodetector.

shaping the optical comb, this device can achieve high angular resolution and a wide range of beam steering angles with minimal beam squint.

The MZM modulates the microwave signal using the Non-Return-to-Zero (NRZ) format onto the FC, then transmits it through a fiber experiencing MI [17], [66], [67].

The FC's flatness plays a pivotal role in achieving optimal performance enhancements in wireless systems based on photonics. A wave-shaper can adjust the distribution of power among the carriers within the FC, leading to a more uniform profile.

In this approach, the scheme permanently assigns frequencies $f_1, f_2, \ldots, f_M$ to antenna elements $1, 2, \ldots,$ and M, respectively, with a free spectral range (FSR) of 200 GHz.

The RF TTD-based signal, utilizing an integrated optical comb source, is transmitted over an optical fiber switching controller system concerning the desired frequency band required for specific wireless communication applications. This MI-based Control system utilizes four optical fibers under MI to cover four different frequency bands. Each fiber is selected with the specific β_2 based on the corresponding frequency.

In the next stage, a programmable bit-control system modifies the length of the positive group velocity dispersion of fiber to offset the delay caused by MI. This system effectively manages and controls the antenna beam by ensuring that it is accurately directed and maintained.

At the BS, the transmitted modulated optical signals are separated into individual wavelengths and converted into RF signals through photodetection.

IV. Architecture of Control Systems

Two distinct control systems are in place: one designed to address the MI phenomenon and the other tailored for managing the beam pattern.

In (9), it is theoretically demonstrated that by adjusting only the parameter β_2, while keeping the carrier power and fiber loss factor constant, the amplified frequency band can be tailored to meet specific requirements.

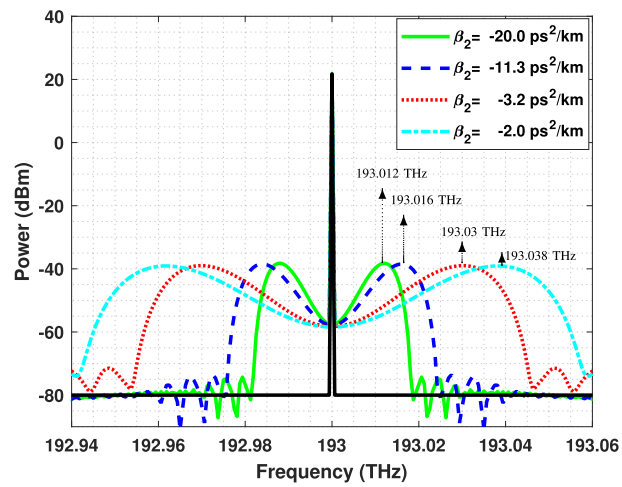

Fig. 5. The carrier sideband amplification by different group velocity dispersion (β_2) of the fiber with 45 km length.

The MI-based switching control system, illustrated in Fig. 4, employs fibers with varying dispersion characteristics. Switches 00, 01, 10, and 11 correspond to fibers with group velocity dispersions of $\beta_2 = -20, -11.3, -3.2$, and -2 ps^2/km, respectively. This system is utilized to amplify different frequency bands with central frequencies of 12, 16, 30, and 38 GHz, as depicted in Fig. 5. Therefore, the modulated signals pass through the desired fiber with respect to their frequency bands. This amplification is related to the frequency, carrier power, and fiber parameters. Then, the control system selects the fiber according to the desired frequency band.

Therefore, this system can accommodate various wireless communication applications across different frequency bands. By leveraging the flexibility the MI-based switching control system provides, the communication infrastructure can be tailored to each application's specific requirements, ensuring optimal performance and efficiency.

The TTD provided by the FC under MI phenomenon with an FSR of 200 GHz ($\Delta\lambda = 1.6$ nm) and a fiber length of 45 km is

calculated as $\Delta\tau = |D_{mi}L_{mi}|\Delta\lambda$, surpassing the required time delay for the antenna. To address this discrepancy, the beam-controller system integrates positive group velocity dispersion ($\beta > 0$) of fiber to mitigate the excess time delay.

If we assign wavelengths $\lambda_1, \lambda_2, \ldots, \lambda_n$ with a narrow spacing of $\Delta\lambda$, we can assume that they all have the same dispersion parameter, D.

The relation between the total value of the TTD and the length of the fibers can be expressed as follows:

$$\Delta\tau = (|D_{mi}L_{mi}| - |D_cL_c|)\Delta\lambda \tag{13}$$

where D_{mi} and L_{mi} represent the dispersion and the length of the fibers affected by MI, while D_c and L_c denote the dispersion and length of standard fibers ($\beta_2 > 0$) employed in the beam-controller system.

It is evident from (13) that there are two manners to adjust the steering angle. The first method involves manipulating the FSR ($\Delta\lambda$). By adjusting the FSR, the spacing between the frequency components of the input signal can be modified, thereby influencing the output of the PAA. The second method of controlling the beam in a PAA is by varying the length of the optical fiber. Changing the fiber length allows the effective path length traveled by the optical signals within the PAA to be adjusted. This alteration in path length directly impacts the time delay experienced by the signals, consequently affecting their interaction and output behavior within the PAA [14], [68]. Both control methods offer distinct advantages and may be employed based on the application's specific requirements. However, adjusting the fiber length is often favored for its simplicity and ease of implementation in practical systems.

Avoiding time delay is also possible by considering $|D_{mi}L_{mi}| = |D_cL_c|$. Therefore, we have developed a configurable dispersion matrix to achieve precise control over the time delay introduced by the fiber under MI.

Employing a fiber with positive group velocity dispersion ($\beta > 0$) effectively mitigates excessive time delays within PAA while also allowing us to regulate time delay by fine-tuning the minimum time delays [69], [70]. Through this approach, the programmable dispersion matrix comprises optical switch devices and dispersive fibers, as depicted in Fig. 4 with four bits. Following this, the comb line undergoes photo-detection and de-multiplexing processes.

By assuming $|D_c| = |D_{mi}| = 1.7\ \frac{ps}{nm.km}$, and $L_{mi} = 45\ km$, the minimum fiber length required in bit-controler system is $L_{min} = 3\ km$. Therefore, the minimum time delay can be set as $\Delta\tau = 8.2\ ps$.

Fig. 6 illustrates the time delay condition for PAA, determined based on the minimum time delay mentioned earlier. By adjusting the binary code, we can modify and regulate the time delay to direct the main beam of PAA.

The directional orientation of an array antenna's beam is dictated by various design characteristics, prominently the wavelength of the operational frequency and the separation between its individual elements, denoted as $d = \lambda/2$. Determining the beam angle is crucial for optimizing antenna performance in telecommunications and satellite communication systems applications.

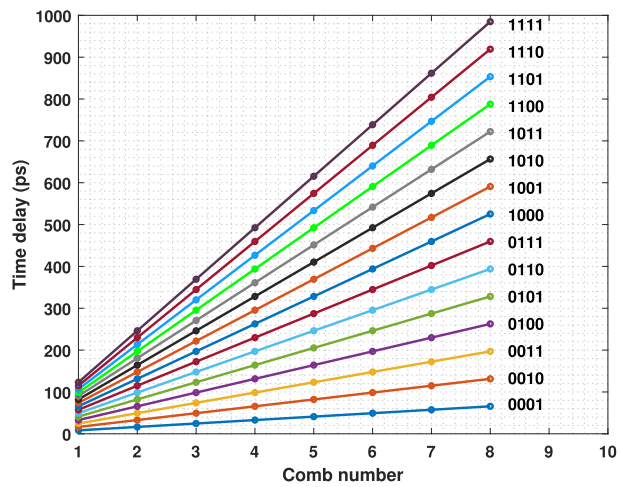

Fig. 6. The value of TTD of the comb lines under the bit-control system, covering states from "0001" to "1111".

The beam angle of an array antenna can be precisely quantified using a formula derived from its design parameters. This formula calculates the angle at which the antenna's beam is focused, providing insights into its coverage pattern and efficiently directing its signal transmission or reception. The formula for calculating the radiating steering angle (θ_0) of an array antenna is as follows:

$$\Theta_0 = \sin^{-1}\frac{c.\Delta\tau}{d} \tag{14}$$

where c and $\Delta\tau$ represent the speed of light in a vacuum and the time delay, respectively.

V. TTD-Based Beamforming

PAAs play a crucial role in enhancing communication performance in wireless applications by dynamically steering RF beams. Traditional beamforming techniques often rely on phase shifting to control the direction of the beam. However, employing TTD in beamforming offers distinct advantages, particularly in wireless scenarios [71].

Firstly, TTD beamforming provides greater flexibility in beam steering compared to phase shift-based methods. By introducing precise delays to the signals at each antenna element, TTD enables the formation of beams with arbitrary angles and shapes. This flexibility is especially advantageous in dynamic environments where the angle of arrival of signals may vary rapidly or the antenna array needs to adapt to changing propagation conditions. Thus, TTD-based beamforming enhances the adaptability and robustness of wireless communication systems, ensuring reliable connectivity in challenging scenarios [72], [73]. Moreover, TTD beamforming improves performance in mitigating interferences and enhancing signal reception. By adjusting the time delays of individual antenna elements, TTD beamforming can optimize the spatial filtering characteristics of the array, effectively suppressing unwanted signals and enhancing the reception of desired signals. This capability is particularly beneficial in crowded wireless environments where multiple signals, such as urban areas or dense networks, may

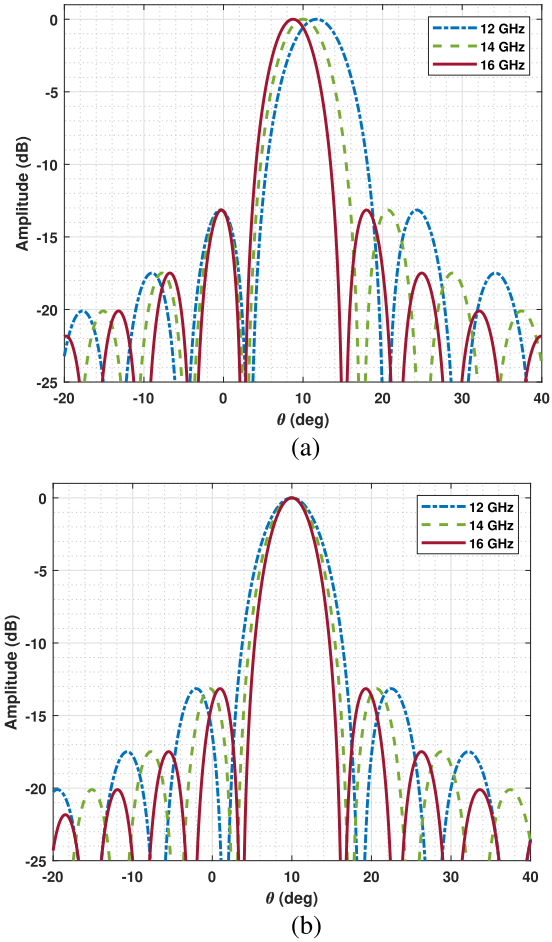

Fig. 7. Comparing array factors across three distinct frequencies, each directed to a 10-degree angle through (a) phase shifting and (b) TDD methods.

overlap. TTD-based beamforming enables efficient utilization of the available spectrum. It enhances wireless communication systems' overall capacity and reliability, ultimately improving the user experience and enabling the deployment of advanced wireless services [74], [75].

The expression for the array factor $G_a(\theta, \lambda)$ of an array steered with phase shifters is as follows [76]:

$$G_a(\theta, \lambda) = \frac{\sin^2[M\pi d(\sin\Theta/\lambda - \sin\Theta_0/\lambda_0)]}{M^2 \sin^2[\pi d(\sin\Theta/\lambda - \sin\Theta_0/\lambda_0)]} \tag{15}$$

where θ and M signify the angle of interest and the number of antenna elements, respectively. This equation allows for the precise calculation of the antenna array's performance. The terms θ_0 and λ_0 serve as reference angles and wavelengths, respectively, offering a baseline for comparative analysis.

In Fig. 7(a), the array factor for a PAA with 16 radiation elements (M = 16) is plotted for three different frequencies of 12, 14, and 16 GHz. Phase shifter settings were determined relative to a center frequency of 14 GHz. It's notable how the beam's position shifts with varying frequencies when utilizing the phase shifter method for steering. On the other hand, when the system uses TTD, the expression for the array pattern is as follows [76]:

$$G_a(\theta, \lambda) = \frac{\sin^2[M\pi(d/\lambda)(\sin\Theta - \sin\Theta_0)]}{M^2 \sin^2[\pi(d/\lambda)(\sin\Theta - \sin\Theta_0)]} \tag{16}$$

The array factor plot, depicted in Fig. 7(b), illustrates the behavior across the same three frequencies mentioned earlier. Notably, all beams are directed towards a fixed angle of 10°.

The plots depicted in Fig. 7 illustrate the advantages of TTD-based beam steering: it enables the accommodation of wide instantaneous bandwidths without experiencing beam squint. This feature holds significant value, especially in applications where resolution enhancement is sought with broader bandwidths.

The angle of the main beam in PAAs can be accurately determined by the value of time delay obtained from the bit-control system, as expressed in (14). To achieve precise control over the array antenna patterns, we explore the manipulation of time delays through binary switches. By adjusting these time delays, we can steer the main beam of the array antenna.

The minimum time delay, as mentioned earlier, is 8.2ps and binary switches with 4-bit configurations provide 16 unique states, as depicted in Fig. 6. Therefore by considering a binary switch with control sequences of '0001', '0010', and '0011', which correspond to time delays of 8.2ps, 16.4ps, and 24.6ps, respectively, the beam angles can be 13.27°, 26.54°, and 39.81°, respectively.

VI. MI-Based Frequency Comb

In our proposed approach, we exploit MI to generate a boosted FC that enhances the performance of RoF systems, particularly when integrated with PAAs. These indicate that the enhancements achieved through MI in the single CW can be applied to systems powered by an FC source. One potential application of this technology is to alleviate the issues of low response of MZM and high signal loss in high-frequency signals used in wireless communications.

Fig. 8 illustrates the boosted FC generated by the MI-based technique, showcasing the equidistant spectral lines resulting from the MI phenomenon. As mentioned in section III, MMR is used to create an FC source with FSR = 200 GHz. These combs' sidebands are amplified through 30 km fiber under MI with group velocity dispersion of $\beta_2 = -20$ ps^2/km. This process occurs alongside MI-based switching utilizing a binary code of 11, effectively amplifying the frequency band centered at 12 GHz. With an input power of 200 mW, the maximum MI gain reaches approximately 18 dB.

The simulation results (Fig. 8(a)) confirm the benefits of utilizing MI-based FC, including enhanced signal quality, improved spatial resolution, and dynamic frequency allocation capabilities. Moreover, the measurements (Fig. 8(b)) validate the feasibility of implementing our approach in practical RoF systems, paving the way for next-generation wireless communication technologies with improved performance and reliability.

The range of fiber length that can be used without signal degradation due to nonlinear effects depends on various factors such as the type of fiber, signal power, signal frequency, and modulation type. This range may vary for each system and

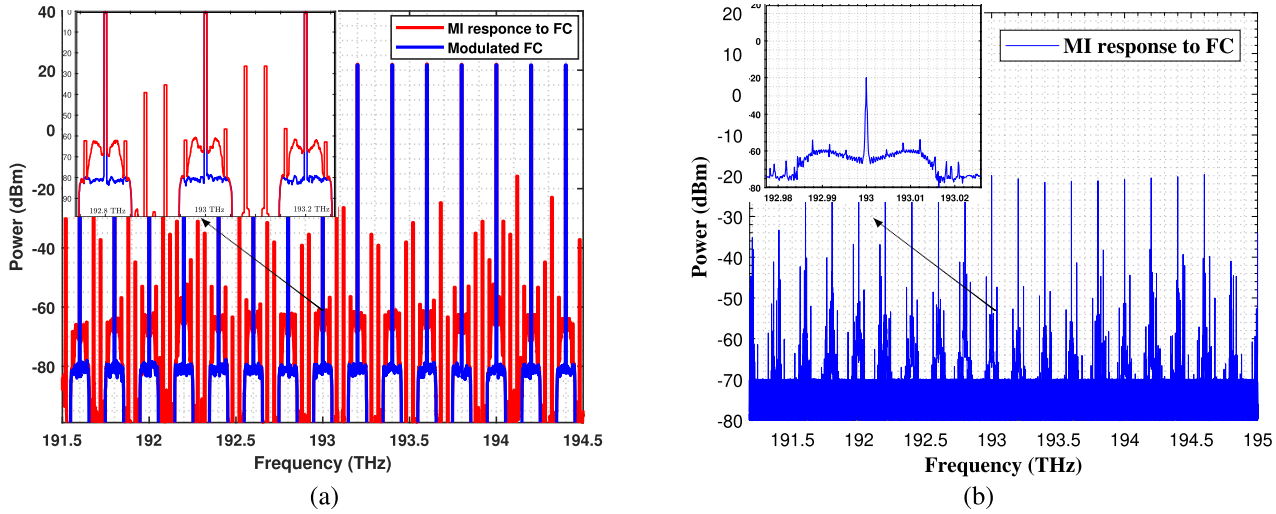

Fig. 8. (a) Simulation and (b) experimental results of MI response to FC by fiber lengths of 30 km with a central frequency of 12 GHz.

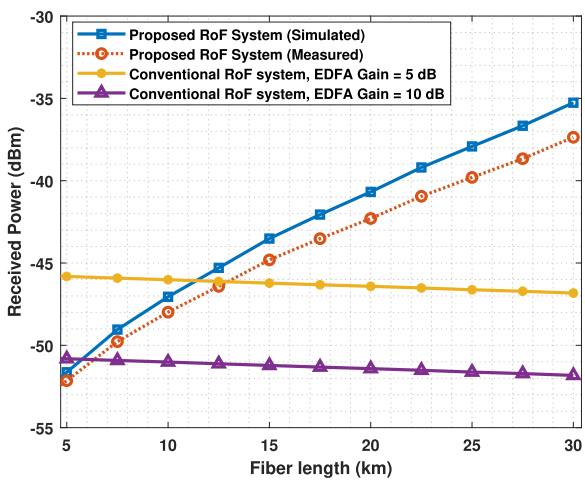

Fig. 9. Variation of received power with fiber length for proposed RoF system without EDFA and conventional RoF system with different values of EDFA gain, 5 dB, and 10 dB.

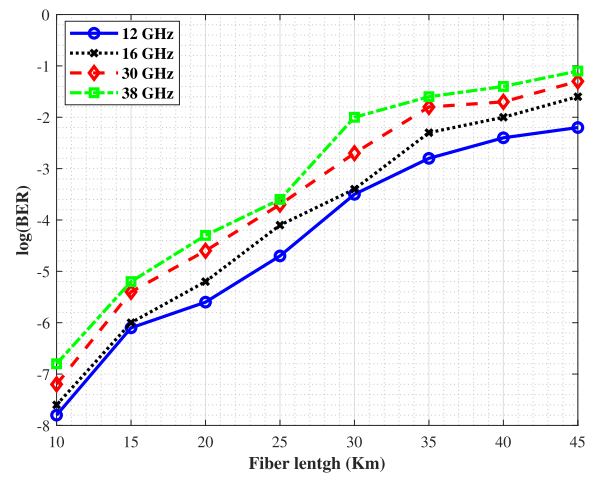

Fig. 10. BER in four different RF frequencies over fiber length.

technology. However, in the "linear region" range, nonlinear effects typically remain limited and controllable, and signal degradation does not occur.

In most of the conventional RoF systems that utilize normal fiber in their structures, the received power decreases with the length of the optical fiber. Therefore, while external amplifiers like EDFA may prove beneficial, the proposed model achieves this amplification through the utilization of the MI phenomenon in fiber optics [77], [78]. Eliminating external devices reduces costs and increases the system's efficiency. This model improves communication networks, especially in long-distance applications.

In order to demonstrate this point, as shown in Fig. 9, we analyze and compare the carrier sideband power based on fiber length in two different RoF systems for 1) in a conventional system with an external amplifier and 2) in the proposed model without an external amplifier.

Fiber parameters in the proposed model are the same in Fig. 2(a) with $\beta_2 = -20\,\mathrm{ps}^2/\mathrm{km}$ and γ at $0.45\,W^{-1}/km$, and for conventional RoF system $\beta_2 = +20\,\mathrm{ps}^2/\mathrm{km}$. The attenuation of both systems is 0.2 dB/km. We demonstrated the desired power could be achieved using the proposed model for long-distance applications without any external amplifier (like the EDFA). As a result, it helps to reduce the cost of wireless systems. The received power in typical RoF systems reduces as the optical fiber's length increases. However, the MI phenomenon can be used to enhance the performance of this system by extending the fibers.

Also, Fig. 10 illustrates the BER at different fiber lengths. BER is plotted for four different RF frequencies on a logarithmic scale: 12, 16, 30, and 38 GHz. The graph shows that up to 45 km of optical link, the BER value lies on a negative axis, which means low transmission error. The BER approaches can be estimated at large distances as a significant transmission error.

Finally, based on the required maximum gain, and by keeping away the signal from distortion, the V_π of MZM and also the PAAs performance is enhanced. Table I shows the gain and

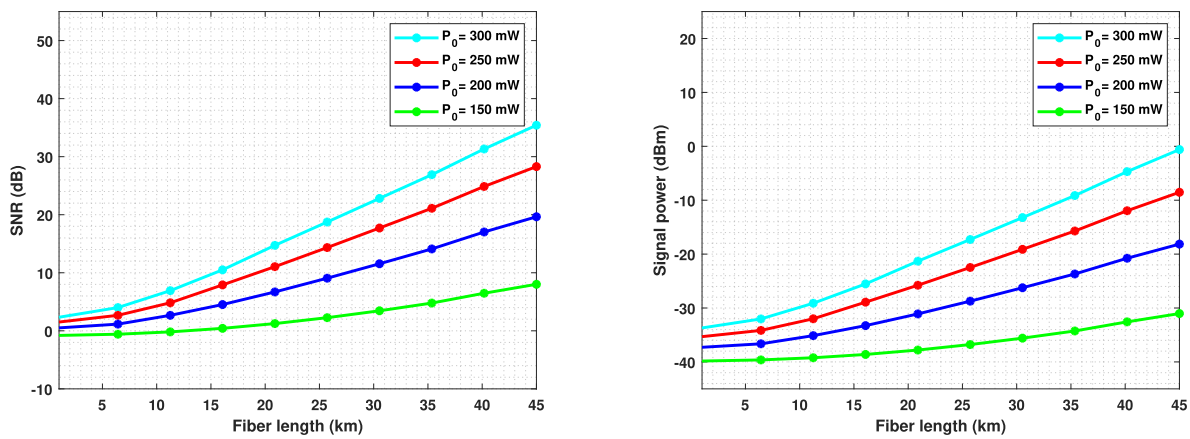

(a) (b)

Fig. 11. Output (a) signal power and (b) SNR vs fiber length for different input power.

TABLE I
PROPOSED ROF SYSTEM RESULT

$f(GHz)$	$\beta_2(ps^2/km)$	$L(km)$	$Gain(dB)$	$Received\ Power(dBm)$	$V_{\pi,eff}$
10-14	-20	1	0.84	-63.5	$\propto 0.9V_\pi$
10-14	-20	15	12.6	-51.4	$\propto 0.23V_\pi$
10-14	-20	30	26.7	-37.3	$\propto 0.046V_\pi$
10-14	-20	45	38.1	-25.9	$\propto 0.012V_\pi$
14-18	-11.3	45	38.1	-25.9	$\propto 0.012V_\pi$
28-32	-3.2	45	38.1	-25.9	$\propto 0.012V_\pi$
36-40	-2.0	45	38.1	-25.9	$\propto 0.012V_\pi$

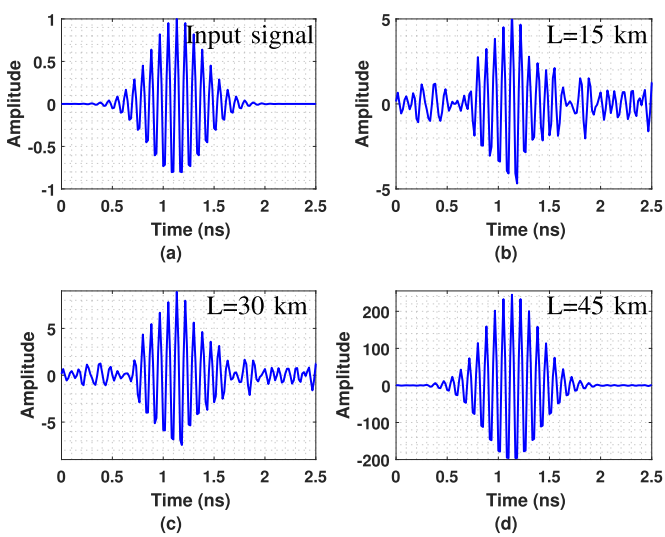

Fig. 12. Shot noise effect on the (a) input RF signal with proposed structure by the different fiber length and with the amount of SNR (b) 12.6 dB, (c) 26.7 dB, and (d) 38.1 dB.

improvement of V_π upon fiber features and the frequency, where the acquired gain is by almost 38.1 dB, and we achieve over 70 times reduction in V_π. The input power, in this case, is -6 dBm.

VII. SNR IN ROF SYSTEM

The random variation in the appearance of electrons and holes at the device's output side causes shot noise in a communication channel. Three approaches can be used to explain shot noise: I) statistical analysis employing Schottky's original premises, II) semiclassical explanation of photodiode detection, and finally, III) completely quantum mechanical treatment of photodetection. According to the original definition, the cathode of a vacuum tube would emit electrons at random, causing current variations with the mean squared value of:

$$< i_{sh}^2 >= 2qi_{dc}\Delta f \tag{17}$$

where q, i_{dc}, and Δf are the elementary charge constant, the DC current, and the bandwidth, respectively.

The formula commonly used to define shot noise is (17). Such a photodiode functions as a traditional square-law device and can convert optical power into electrical power with reasonable efficiency. The corresponding photocurrent for an incident optical field E(t) is $I(t) = \Re A(\epsilon/\mu)^{1/2}|E(t)|^2/2$, where $\Re$ is the photodiode responsivity in units of A/W, where μ is the fiber core permittivity, A is the cross-sectional area of the fiber mode, and ϵ is the fiber core permeability.

Therefore, the DC photocurrent sourced from a p–i–n junction illuminated by an average optical power $< P_{opt} >$ is

$$i_{dc} = \Re < P_{opt} > \tag{18}$$

This expression assumes Specific quantum efficiency for the power transfer from the fiber core to the photodiode. It is essential to note that, between the fiber and the photodiode absorption zone, when the structure is lossless, the responsivity becomes an "effective responsivity" $\Re_{eff}$, where $\Re_{eff} = \frac{\eta q}{hw}$. With using

(17) and (18) we have [79] :

$$<i_{sh}^2>=\frac{2\eta q^2}{hw}<P_{opt}>\Delta f \tag{19}$$

(19) is semiclassical in the sense that it employs quantization of the electron charge (q) and the photon energy (hw).

Therefore, the shot-noise power due to the photodetector is directly proportional to the input power. In some cases, when the signal power level is very low, or even when it is near the level of shot noise power, detecting the signal is very difficult since the noise power and input power increase simultaneously. When the fiber length increases, the signal can be amplified separately while the noise power remains constant by utilizing the MI of optical fiber. Furthermore, the SNR in photonic microwave structures is proportional to the inverse square of the $V_{\pi,eff}$, which improves the SNR due to its reduction and channel capacity [56].

$$SNR=\frac{PP_{RF,in}Z_mR_d}{4q\Delta f}\frac{\pi^2}{V_{\pi,eff}^2} \tag{20}$$

where Z_m is the electrical impedance of the modulator, R_d is the photodetector responsivity expressed as the ratio of the photo-generated electrical current divided by the incident optical power. Therefore, by increasing the gain and improving the voltage of the modulator, the effect of noise decreases.

Fig. 11 illustrates the output signal power and SNR vs fiber length for different carrier power. In fact, by increasing the input power or fiber length, the gain or SNR can be improved. It is essential to note that we can achieve the same gain or SNR with a longer fiber length to recompense the effect of the lower power of the laser.

Now, we investigate sending a weak signal despite the shot noise generated by the photodetector. Fig. 12(a) shows the normalized RF input signal modulated on the carrier with a power of 300 mW. By increasing the length of the fiber, the signal is amplified and can be distinguished from noise. It should be noted that the nonlinear effect is small enough not to affect the signal's amplitude.

Fig. 12 illustrates how the shot noise effect decreases as the fiber length increases to 15 km, 30 km, and 45 km. In this case, the RoF system response with a Gaussian pulse is displayed, and the photodetector experiences shot noise at a power level of −36 dBm. Increasing the fiber length enhances the MI gain, leading to a significant reduction in the noise effect.

VIII. Conclusion

This paper demonstrates the significant potential of RoF systems wireless communication technology contribution. By leveraging the MI phenomenon and MI-based control system architecture, RoF systems can enhance the performance of PAA across diverse frequency bands. The experimental results validate the feasibility and effectiveness of the proposed approach, showcasing MI gains of 18 dB through 30 km fiber under MI. The proposed RoF system features RF signals with central frequencies ranging from 12 to 38 GHz and traverses fibers ranging from 1 km to 45 km in length, resulting in MI gains ranging from 0.84 dB to 38.1 dB, respectively. Unlike conventional systems, the system's gain increases as the fiber's length increases. Notably, employing a 45 km fiber, the system achieves over 70 times V_π reduction. Therefore, the proposed structure is a good candidate for wireless communication systems.

References

[1] E. Nazemosadat, J. I. Herranz-Herruzo, and I. Gasulla, "Phased array antenna beam-steering in a dispersion-engineered few-mode fiber," *J. Lightw. Technol.*, vol. 41, no. 21, pp. 6651–6656, Nov. 2023.

[2] D. Che, "Analog vs digital radio-over-fiber: A spectral efficiency debate from the SNR perspective," *J. Lightw. Technol.*, vol. 39, no. 16, pp. 5325–5335, Aug. 2021.

[3] S. Rommel et al., "Real-time high-bandwidth mm-wave 5G NR signal transmission with analog radio-over-fiber fronthaul over multi-core fiber," *EURASIP J. Wireless Commun. Netw.*, vol. 2021, no. 1, pp. 1–20, 2021.

[4] A. Delmade et al., "Optical heterodyne analog radio-over-fiber link for millimeter-wave wireless systems," *J. Lightw. Technol.*, vol. 39, no. 2, pp. 465–474, Jan. 2021.

[5] C. Wang et al., "High-speed terahertz band radio-over-fiber system using hybrid time-frequency domain equalization," *IEEE Photon. Technol. Lett.*, vol. 34, no. 11, pp. 559–562, Jun. 2022.

[6] F. M. Al-Zubaidi, J. L. Cardona, D. S. Montero, and C. Vazquez, "Optically powered radio-over-fiber systems in support of 5G cellular networks and IoT," *J. Lightw. Technol.*, vol. 39, no. 13, pp. 4262–4269, Jul. 2021.

[7] J. D. López-Cardona et al., "Power-over-fiber in a 10 km long multicore fiber link within a 5G fronthaul scenario," *Opt. Lett.*, vol. 46, no. 21, pp. 5348–5351, 2021.

[8] M. Sung et al., "Photonic THz communications based on radio-over-fiber technology for 6G mobile network: Design and opportunity," *IEEE J. Sel. Topics Quantum Electron.*, vol. 29, no. 5, Sep.-Oct. 2023, Art. no. 8600611.

[9] S. A. Khorasani, H. Zakeri, G. Moradi, M. Alibakhshikenari, C. H. See, and E. Limiti, "Orbital angular momentum with the approach of using in sub-6 GHz 5G mobile communications for wireless applications," in *2024 6th Glob. Power Energy Commun. Conf.*, 2024, pp. 1–4.

[10] D. F. Paredes-Páliz, G. Royo, F. Aznar, C. Aldea, and S. Celma, "Radio over fiber: An alternative broadband network technology for IoT," *Electronics*, vol. 9, no. 11, 2020, Art. no. 1785.

[11] N. Chen and M. Okada, "Toward 6G Internet of Things and the convergence with ROF system," *IEEE Internet Things J.*, vol. 8, no. 11, pp. 8719–8733, Jun. 2021.

[12] S.-R. Moon, M. Sung, E.-S. Kim, J. K. Lee, S.-H. Cho, and J. Kim, "RoF-based indoor distributed antenna system that can simultaneously support 5G mmwave and 6G terahertz services," *Opt. Exp.*, vol. 30, no. 2, pp. 1521–1533, 2022.

[13] S. Cho, S.-R. Moon, M. Sung, S.-H. Cho, T. Kawanishi, and H.-J. Song, "A 262-GHz wireless IFoF uplink with remote down-conversion using optically generated sub-THz LO," *IEEE Trans. Microw. Theory Techn.*, vol. 71, no. 5, pp. 2276–2285, May 2023.

[14] R. Azizpour, H. Zakeri, and G. Moradi, "Beam pattern control for graphene-based patch array antenna with radio-over-fiber systems by using modulation instability phenomenon," *Opt. Continuum*, vol. 2, no. 4, pp. 865–876, 2023.

[15] S. Conombo, M. D. Diouf, S. Ouya, and A. D. Kora, "Radio signal generation over fiber by optical injection locking," in *2020 22nd Int. Conf. Adv. Commun. Technol.*, 2020, pp. 430–436.

[16] S. Islam, M. F. Khan, M. Z. Hossan, and M. A. Amin, "An overview of radio over fiber (RoF) technology," in *2019 2nd Int. Conf. Intell. Comput. Instrum. Control Technol.*, 2019, vol. 1, pp. 749–752.

[17] H. Khalil et al., "Performance analysis of modulation formats for next generation RoF systems," *IEEE Access*, vol. 9, pp. 139393–139402, 2021.

[18] H. Ji, C. Sun, and W. Shieh, "Spectral efficiency comparison between analog and digital RoF for mobile fronthaul transmission link," *J. Lightw. Technol.*, vol. 38, no. 20, pp. 5617–5623, Oct. 2020.

[19] I. A. Rather, G. Kumar, and R. Saha, "Survey on RoF technology and the mitigation schemes over the challenges in the RoF network," *Optik*, vol. 247, 2021, Art. no. 168007.

[20] C.-C. Wei, C.-T. Lin, H.-T. Huang, W.-L. Liang, and S. Chi, "Estimation and suppression of dispersion-induced phase noise in w-band direct-detection OFDM radio-over-fiber systems," *J. Lightw. Technol.*, vol. 32, no. 20, pp. 3874–3884, Oct. 2014.

[21] J. P. Santacruz, S. Rommel, U. Johannsen, A. Jurado-Navas, and I. T. Monroy, "Analysis and compensation of phase noise in mm-wave OFDM ARoF systems for beyond 5G," *J. Lightw. Technol.*, vol. 39, no. 6, pp. 1602–1610, Mar. 2021.

[22] R. M. Mahmood, S. Yaakob, F. A. Ahmad, S. B. A. Anas, M. Z. A. Kadir, and M. R. C. Beson, "Effect of phase noise on the optical millimeter-wave signal in the DWDM-RoF system," *Electronics*, vol. 11, no. 3, 2022, Art. no. 489.

[23] M. K. Asif Khan et al., "Mitigation of phase noise and nonlinearities for high capacity radio-over-fiber links," *Electronics*, vol. 10, no. 3, 2021, Art. no. 345.

[24] Y. Shu, H. J. Qian, X. Gao, and X. Luo, "A low phase noise and high FoM distributed-swing-boosting multi-core oscillator using harmonic-impedance-expanding technique," *IEEE J. Solid-State Circuits*, vol. 56, no. 12, pp. 3728–3740, Dec. 2021.

[25] A. J. Seeds and K. J. Williams, "Microwave photonics," *J. Lightw. Technol.*, vol. 24, no. 12, pp. 4628–4641, Feb. 2006.

[26] D. Eliyahu, D. Seidel, and L. Maleki, "RF amplitude and phase-noise reduction of an optical link and an opto-electronic oscillator," *IEEE Trans. Microw. Theory Techn.*, vol. 56, no. 2, pp. 449–456, Feb. 2008.

[27] A. A. Sabri, S. M. Hameed, and W. A. Hadi, "Last mile access-based FSO and VLC systems," *Appl. Opt.*, vol. 62, no. 31, pp. 8402–8410, 2023.

[28] S. Sachdeva, H. Pahuja, M. Sindhwani, S. Kaur, A. Kumar, and M. K. Shukla, "Composition distribution matching (CCDM) encoded 32-QAM-RoF system supporting 100 GHz radio signal," *J. Opt.*, vol. 53, pp. 2679–2686, 2023.

[29] I. García López et al., "High speed bicmos linear driver core for segmented INP Mach-Zehnder modulators," *Analog Integr. Circuits Signal Process.*, vol. 87, pp. 105–115, 2016.

[30] W. Yao, G. Gilardi, M. K. Smit, and M. J. Wale, "Performance degradation of integrated optical modulators due to electrical crosstalk," *J. Lightw. Technol.*, vol. 34, no. 13, pp. 3080–3086, Jul. 2016.

[31] G. K. Gopalakrishnan, W. K. Burns, R. W. McElhanon, C. H. Bulmer, and A. S. Greenblatt, "Performance and modeling of broadband LiNbO/sub 3/traveling wave optical intensity modulators," *J. Lightw. Technol.*, vol. 12, no. 10, pp. 1807–1819, Oct. 1994.

[32] D. A. Presti, V. Guarepi, F. Videla, A. Fasciszewski, and G. A. Torchia, "Intensity modulator fabricated in LiNbO3 by femtosecond laser writing," *Opt. Lasers Eng.*, vol. 111, pp. 222–226, 2018.

[33] A. Rueda, F. Sedlmeir, M. Kumari, G. Leuchs, and H. G. Schwefel, "Resonant electro-optic frequency comb," *Nature*, vol. 568, no. 7752, pp. 378–381, 2019.

[34] H. Mahrous et al., "Design of compact, high-speed and low-loss silicon-on-silica electro-optic modulators," *Semicond. Sci. Technol.*, vol. 35, no. 9, 2020, Art. no. 095017.

[35] H. Gevorgyan, A. Khilo, Y. Ehrlichman, and M. A. Popović, "Triply resonant coupled-cavity electro-optic modulators for RF to optical signal conversion," *Opt. Exp.*, vol. 28, no. 1, pp. 788–815, 2020.

[36] H. Hwang et al., "Hyperband electro-optic modulator based on a two-pulley coupled lithium niobate racetrack resonator," *Opt. Lett.*, vol. 49, no. 3, pp. 658–661, 2024.

[37] C. Ziółkowski, J. M. Kelner, J. Krygier, A. Chandra, and A. Prokeš, "Radio channel capacity with directivity control of antenna beams in multipath propagation environment," *Sensors*, vol. 21, no. 24, 2021, Art. no. 8296.

[38] T. Chaloun et al., "Electronically steerable antennas for future heterogeneous communication networks: Review and perspectives," *IEEE J. Microw.*, vol. 2, no. 4, pp. 545–581, Oct. 2022.

[39] L. Galdino et al., "Optical fibre capacity optimisation via continuous bandwidth amplification and geometric shaping," *IEEE Photon. Technol. Lett.*, vol. 32, no. 17, pp. 1021–1024, Sep. 2020.

[40] S. Ogurtsov, D. Caratelli, and Z. Song, "A review of synthesis techniques for phased antenna arrays in wireless communications and remote sensing," *Int. J. Antennas Propag.*, vol. 2021, pp. 1–20, 2021.

[41] B. Zheng, C. You, W. Mei, and R. Zhang, "A survey on channel estimation and practical passive beamforming design for intelligent reflecting surface aided wireless communications," *IEEE Commun. Surv. Tut.*, vol. 24, no. 2, pp. 1035–1071, Secondquarter 2022.

[42] W. Hong et al., "The role of millimeter-wave technologies in 5G/6G wireless communications," *IEEE J. Microw.*, vol. 1, no. 1, pp. 101–122, Jan. 2021.

[43] J. Kaur et al., "Contextual beamforming: Exploiting location and AI for enhanced wireless telecommunication performance," *APL Mach. Learn.*, vol. 2, no. 1, 2024, Art. no. 016113.

[44] X. Wang et al., "Optical true time delay-based hybrid beamforming for limited-feedback millimeter-wave massive MIMO systems," *IEEE Commun. Lett.*, vol. 25, no. 7, pp. 2405–2409, Jul. 2021.

[45] D. W. Prather et al., "Fourier-optics based opto-electronic architectures for simultaneous multi-band, multi-beam, and wideband transmit and receive phased arrays," *IEEE Access*, vol. 11, pp. 18082–18106, 2023.

[46] I. F. Akyildiz, C. Han, Z. Hu, S. Nie, and J. M. Jornet, "Terahertz band communication: An old problem revisited and research directions for the next decade," *IEEE Trans. Commun.*, vol. 70, no. 6, pp. 4250–4285, Jun. 2022.

[47] H. Yerranna, K. S. Kumar, and S. L. Sabat, "Phase noise modeling and experimental demonstration of single and dual-loop direct modulation optoelectronic oscillator," *IEEE J. Quantum Electron.*, vol. 58, no. 6, Dec. 2022, Art. no. 5000210.

[48] F. Monet, J.-S. Boisvert, and R. Kashyap, "A simple high-speed random number generator with minimal post-processing using a random Raman fiber laser," *Sci. Rep.*, vol. 11, no. 1, 2021, Art. no. 13182.

[49] P. Yupapin, A. Sharafali, P. Sreethu, T. Sridarshini, D. Adhikari, and M. Karthikeyan, "Modulation instability induced supercontinuum generation in defective core photonic crystal fiber," *Opt. Quantum Electron.*, vol. 54, no. 8, 2022, Art. no. 504.

[50] F. Copie, S. Randoux, and P. Suret, "The physics of the one-dimensional nonlinear schrödinger equation in fiber optics: Rogue waves, modulation instability and self-focusing phenomena," *Rev. Phys.*, vol. 5, 2020, Art. no. 100037.

[51] T. Cheng et al., "Experimental investigation of the polarization modulation instability and stimulated Raman scattering in a chalcogenide optical fiber," *J. Appl. Phys.*, vol. 128, no. 19, 2020, Art. no. 193103.

[52] T. A. Sulaiman, "Three-component coupled nonlinear Schrödinger equation: Optical soliton and modulation instability analysis," *Physica Scripta*, vol. 95, no. 6, 2020, Art. no. 065201.

[53] K. Sozos, S. Deligiannidis, G. Sarantoglou, C. Mesaritakis, and A. Bogris, "Recurrent neural networks and recurrent optical spectrum slicers as equalizers in high symbol rate optical transmission systems," *J. Lightw. Technol.*, vol. 41, no. 15, pp. 5037–5050, Aug. 2023.

[54] Z. Wang, Y. Mao, X. Ling, and L. Zhang, "Nonlinear evolution of modulational instability under the interaction of kerr nonlinearity with pure higher, even-order dispersion," *Opt. Exp.*, vol. 31, no. 25, pp. 42338–42346, 2023.

[55] S. Savotchenko, "Propagation of nonlinear surface waves along the interface between a kerr-type crystal and a medium characterized by stepwise dielectric permittivity," *J. Opt.*, vol. 22, no. 6, 2020, Art. no. 065504.

[56] G. P. Agrawal, *Fiber-Optic Communication Systems*. Hoboken, NJ, USA: Wiley, 2012.

[57] M. Erkintalo et al., "Higher-order modulation instability in nonlinear fiber optics," *Phys. Rev. Lett.*, vol. 107, no. 25, 2011, Art. no. 253901.

[58] A. Adhikary et al., "Performance analysis of Q-factor on wavelengths and bit rates using optical solitons with dispersion management," *J. Opt.*, vol. 49, no. 4, pp. 533–542, 2020.

[59] S. Shimizu et al., "PPLN-based optical parametric amplification for wideband WDM transmission," *J. Lightw. Technol.*, vol. 40, no. 11, pp. 3374–3384, Jun. 2022.

[60] S. A. Madani, M. Bahrami, and A. Rostami, "Multi-clad optical fiber design for ultra-wideband modulation instability," *Physica Scripta*, vol. 97, no. 4, 2022, Art. no. 045501.

[61] G. Wang et al., "Stable and highly efficient free-space optical wireless communication system based on polarization modulation and in-fiber diffraction," *J. Lightw. Technol.*, vol. 39, no. 1, pp. 83–90, Jan. 2021.

[62] Y. Yan et al., "Distributed optical fiber sensing assisted by optical communication techniques," *J. Lightw. Technol.*, vol. 39, no. 12, pp. 3654–3670, Jun. 2021.

[63] P. Mohanraj, R. Sivakumar, and E. E. S. Massoud, "Role of higher order dispersion on instability criterion of saturable fiber system with non-kerr nonlinearities," *Optik*, vol. 253, 2022, Art. no. 168608.

[64] K. K. Qureshi, A. R. Qureshi, M. G. Magam, and L. Jamal, "Radio-over-fiber front-haul link design using optisystem," *J. Opt. Commun.*, vol. 44, 2020, Art. no. 000010151520200074.

[65] J. Golden and D. O' Malley, "Reverse annealing for nonnegative/binary matrix factorization," *Plos One*, vol. 16, no. 1, 2021, Art. no. e0244026.

[66] Z. Ibrahim, C. Rashidi, S. Aljunid, A. Rahman, and M. Anuar, "NRZ and RZ analysis for optical CDMA based on radio over fiber (RoF) technique," in *2016 3rd Int. Conf. Electron. Des.*, 2016, pp. 151–154.

[67] B. Tamrakar, K. Singh, P. Kumar, and S. Shukla, "Performance optimization of conventional RoF link by considering the effect of RF source linewidth and photonic source linewidth for the next-generation networks," *J. Opt.*, vol. 52, no. 4, pp. 2096–2108, 2023.

[68] A. Bekkali, H. Fujita, and M. Hattori, "New generation free-space optical communication systems with advanced optical beam stabilizer," *J. Lightw. Technol.*, vol. 40, no. 5, pp. 1509–1518, Mar. 2022.

[69] P. Zheng et al., "A wideband 1× 4 optical beam-forming chip based on switchable optical delay lines for ka-band phased array," *Opt. Commun.*, vol. 488, 2021, Art. no. 126842.

[70] L. Li et al., "Optical fiber optofluidic bio-chemical sensors: A review," *Laser Photon. Rev.*, vol. 15, no. 7, 2021, Art. no. 2000526.

[71] E. Zeydan, O. Dedeoglu, and Y. Turk, "Experimental evaluations of TDD-based massive MIMO deployment for mobile network operators," *IEEE Access*, vol. 8, pp. 33202–33214, 2020.

[72] C.-C. Lin et al., "Wideband beamforming with rainbow beam training using reconfigurable true-time-delay arrays for millimeter-wave wireless [feature]," *IEEE Circuits Syst. Mag.*, vol. 22, no. 4, pp. 6–25, Fourthquarter 2022.

[73] M. Ali, R. Cruzoe-Guzmán, L. E. Garcia-Muñoz, F. v. Dijk, and G. Carpintero, "Photonics-enabled millimetre-wave phased-array antenna with true time delay beam-steering," in *2020 50th Eur. Microw. Conf.*, 2021, pp. 316–319.

[74] R. M. Vaghefi, R. C. Palat, G. Marzin, K. Basavaraju, Y. Feng, and M. Banu, "Achieving phase coherency and gain stability in active antenna arrays for sub-6 GHz FDD and TDD FD-MIMO: Challenges and solutions," *IEEE Access*, vol. 8, pp. 152680–152696, 2020.

[75] C. Guo, L. Tian, Z. H. Jiang, and W. Hong, "A self-calibration method for 5G full-digital TDD beamforming systems using an embedded transmission line," *IEEE Trans. Antennas Propag.*, vol. 69, no. 5, pp. 2648–2659, May 2021.

[76] X. Xu et al., "Photonic microwave true time delays for phased array antennas using a 49 GHz FSR integrated optical micro-comb source," *Photon. Res.*, vol. 6, no. 5, pp. B30–B36, 2018.

[77] L. Xiao, Y. Wang, Y. Li, Q. Bai, X. Liu, and B. Jin, "Polarization fading suppression for optical fiber sensing: A review," *IEEE Sensors J.*, vol. 22, no. 9, pp. 8295–8312, May 2022.

[78] K. Liu et al., "Interferometer-based distributed optical fiber sensors in long-distance vibration detection: A review," *IEEE Sensors J.*, vol. 22, no. 22, pp. 21428–21444, Nov. 2022.

[79] V. J. Urick, K. J. Williams, and J. D. McKinney, *Fundamentals of Microwave Photonics*. Hoboken, NJ, USA:Wiley, 2015.

Open Access funding provided by 'Università degli Studi di Roma "Tor Vergata"' within the CRUI CARE Agreement